J. Fluid Mech. (1983), *vol.* 133, *pp.* 217–231
Printed in Great Britain

An experimental investigation of laminar axisymmetric submerged jets

By G. W. RANKIN, K. SRIDHAR, M. ARULRAJA AND K. R. KUMAR

Department of Mechanical Engineering, University of Windsor, Windsor, Ontario, Canada

(Received 26 August 1982 and in revised form 7 April 1983)

Detailed measurements of the velocity profiles in a laminar axisymmetric submerged jet of water were taken using a laser-Doppler anemometer. A non-intrusive measurement technique is particularly advantageous in this application owing to the unstable nature of the laminar jet and the destabilizing effect which objects submerged in the jet have. Flow visualization was employed to ensure that all of the measuring points were located within the laminar region of the jet.

The variation of centreline velocity, jet half-radius and velocity-profile shape are investigated for various Reynolds numbers and axial distances. Emphasis is placed on the jet-development region; however, data from the fully developed region are also presented. Particular attention is given to determine the proper non-dimensional groups which are required to collapse the data. The predictions of a simple boundary-layer analysis are used as a guide in this regard and found to give an accurate representation of the flow field.

Velocity-profile data were taken at sufficiently small radial increments to allow a determination of the jet kinematic momentum using the basic integral definition. Although approximately constant, a slight variation with axial distance is indicated. The momentum initially decreases, and then increases gradually to a value greater than that at the tube exit. An attempt to explain the trend of the variation is made using certain hypotheses regarding the velocity and pressure conditions at the tube exit.

1. Introduction

The present investigation was undertaken in order to provide detailed experimental velocity-profile information within the developing region of an axisymmetric laminar submerged jet with a fully developed velocity profile at the tube exit. This apparently simple flow situation has been considered previously by a number of investigators; however, certain important questions regarding the flow field remain unanswered.

Although there is evidence of experimental work being conducted in this area near the turn of this century (see Birkhoff & Zarantonello 1957, p. 274), the work of Andrade & Tsien (1937) is the most often quoted classical work.

Andrade & Tsien used a suspended particle method to determine the velocity profiles within an axisymmetric liquid jet at large axial distances away from the tube exit plane. They were unable to obtain results near the exit of the tube; however, using experimental information further downstream, they inferred that the exit

profile was uniform. Their velocity profiles were shown to agree well with the analytical solution that Schlichting proposed in 1933 (see Schlichting 1968). The axial and radial velocity components u and v are given to be

$$u = \frac{3J}{8\pi\mu}\frac{1}{x_s}\frac{1}{[1+\xi^2]^2}, \tag{1}$$

$$v = \left(\frac{3J}{4\pi\rho}\right)^{\frac{1}{2}}\frac{1}{x_s}\frac{\xi-\xi^3}{[1+\xi^2]^2}, \tag{2}$$

where

$$\xi = \frac{1}{8\nu}\left[\frac{3J}{\pi\rho}\right]^{\frac{1}{2}}\frac{r}{x_s}, \tag{3}$$

J is the axial momentum flux across any plane normal to the axis of the jet, μ the absolute viscosity and ρ the density of the fluid. The distance x_s is measured along the jet axis from the point origin of the jet.

The assumption made in Schlichting's analysis, namely, the constancy of axial momentum flux J and the approximations that pertain to the boundary layer, are substantiated at least at large distances downstream. This region of the jet has become known as the similarity region because of the nature of Schlichting's solution. In order to show the good agreement between theory and experiment it was necessary to shift the position of the point source of the theoretical jet by a distance x_{cv} to a new location referred to as the virtual origin.

Although other point-source models have been proposed by Landau (1944), Squire (1951) and Morton (1967), Schlichting's solution is the one most often applied. This is likely due to its simplicity and proven accuracy and is chosen in spite of the fact that the approaches of Landau and Squire are exact solutions of the Navier–Stokes equation.

Recent experimental investigations of the laminar axisymmetric submerged jet have been conducted by Hrycak *et al.* (1970), Vaz (1970), Symons & Labus (1971), Chang (1972), du Plessis, Wang & Tsang (1973), Abramovich & Solan (1973) and Dmitriev & Kulesova (1974). A deficiency associated with a number of these works is the incomplete coverage that has been given to the developing region of the jet. In certain cases not enough information was presented to allow one to extract the original data from the processed information given. A description of the steps taken to ensure that all of the experimental data originated from a steady laminar jet rather than an unsteady laminar or semiturbulent jet was in many cases vague or non-existent. The inherent instability of a laminar jet is a factor of particular importance to the study of such a flow situation. The unsteady nature of vortices which appear in the free shear layer, and their growth, can significantly affect the flow field in certain regions. For large values of Reynolds numbers the ultimate effect is the transition to turbulence. Analytical models that are available in the literature do not account for such phenomena.

In all of the abovementioned studies the probe used to obtain the measurements was physically in the flow field and hence could act as a flow disturbance. This could cause premature transition to turbulence. In the cases where a hot wire was used, local temperature disturbances would also be imposed.

The determination of the jet axial-momentum flux has not been considered extensively in the available literature. When it is considered, the method of evaluating it is usually based on the form of the similarity solution in the fully developed region (see Andrade & Tsien 1937). Abramovich & Solan (1973), using a

method similar to that mentioned above, concluded that the jet momentum was not conserved in the developing region. They also determined that, in order to collapse the experimental data, $(x/d)\,Re^{-\frac{1}{2}}$ should be used as the non-dimensional axial distance. This conclusion is in disagreement with the result $X_c = (x/d)\,Re_c^{-1}$ that is obtained by using the boundary-layer assumptions with the continuity and momentum equations. In the above, x is the axial distance measured from the tube exit plane, d is the tube diameter, $Re = u_{av}\,d/\nu$ and $Re_c = u_{max}\,d/\nu$, where u_{av} and u_{max} are respectively the average and the maximum velocities at the jet exit.

The boundary-layer equations are the basis for the numerical solutions of the laminar jet presented by Pai & Hsieh (1972), Fox *et al.* (1972), du Plessis *et al.* (1973) and Arulraja (1982). The last reference presents the solution in a convenient tabular manner and is used for comparisons with the present data.

The experimental investigation has been conducted such that each velocity profile includes a sufficient number of data points to allow accurate numerical integration to obtain the kinematic momentum using the basic definition. This enables the method to indicate a variation of the jet momentum in the axial direction within the developing region, unlike any other method available in the literature, and is independent of any assumed form of the velocity profile.

Velocity profiles at various stages of development, for different Reynolds-number and axial-distance combinations, are included in order to determine which non-dimensional axial coordinate is preferable.

Throughout the experiment, extreme precautions are taken to ensure that only a steady laminar jet is being considered. Flow-visualization tests are used for this purpose. In addition, the use of the laser-Doppler anemometer causes the least possible disturbance to the flow. The smallness of the measuring volume and the velocity resolution are additional advantages of the present study.

For each jet considered, the supply tube is of sufficient length to provide a fully developed (parabolic) pipe-flow velocity profile at the tube exit.

2. Experimental equipment

A schematic diagram of the closed-loop flow facility used in the present study is shown in figure 1. Water from the reservoir was pumped to the upstream constant-head tank. The overflow from this tank was returned to the reservoir, and the test fluid passed through a rotameter, flow-regulating valve and settling chamber before entering the supply tube. These items were fastened onto a laboratory table, which was bolted to the floor in order to maintain alignment with the jet chamber and downstream constant-head tank, which were located on another stand, also bolted to the floor, some distance away. The measuring volume of the laser-Doppler anemometer could be positioned at almost any point within the jet chamber using the traverse mechanism upon which it was fastened. The flow from the downstream constant-head tank was returned to the reservoir, at which point it could be either recirculated or directed into a graduated cylinder, and weighed in order to determine the mass-flow rate.

The jet of interest was formed inside the jet chamber, shown schematically in figure 2. The end of the supply tube was flush with the inner wall of the jet chamber. Although the chamber is not infinite in lateral extent, there is little doubt that it is large enough to simulate an unconfined jet, especially in the region just downstream of the tube exit. The chamber was constructed of Plexiglas to allow the laser beams to be positioned as shown. The top plate was covered with black paper except for a

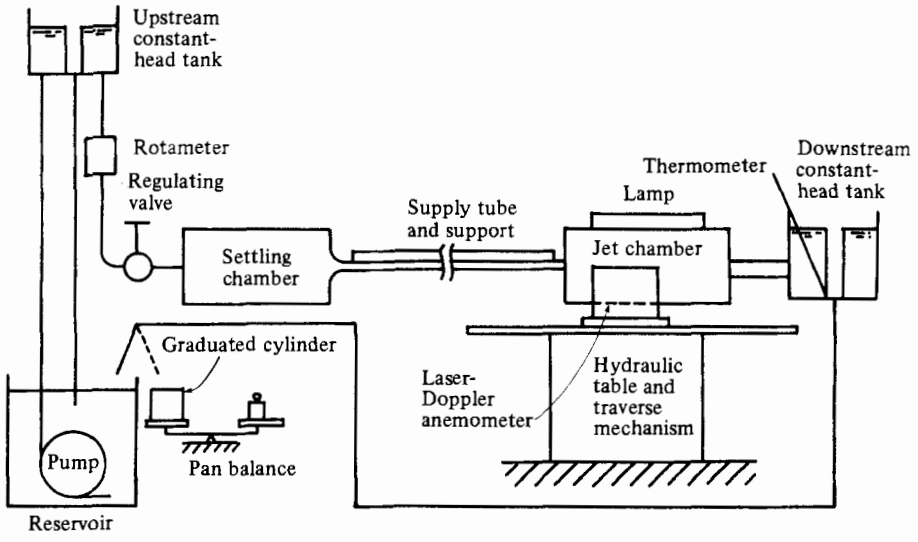

FIGURE 1. Flow test facility.

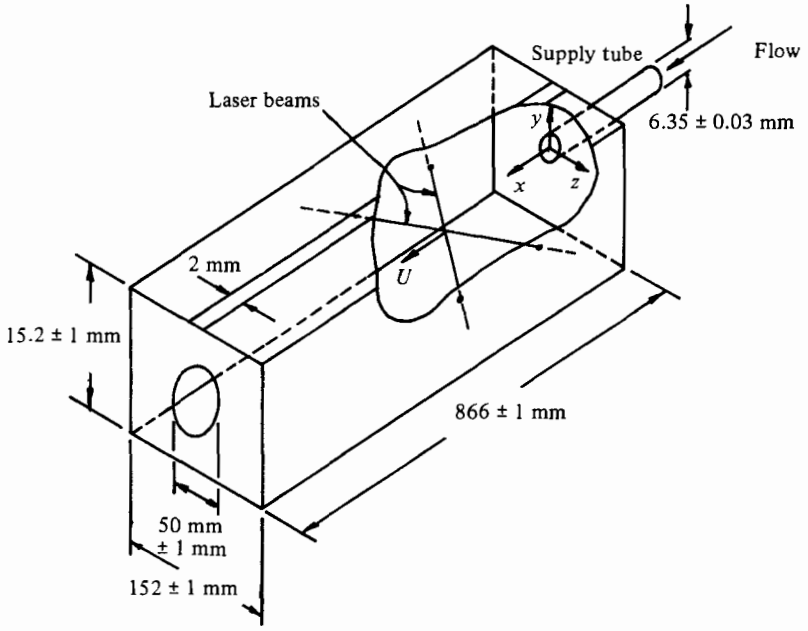

FIGURE 2. Jet receiving chamber.

2 mm wide strip along the centre, and a fluorescent light was positioned above this slit to illuminate the dyed laminar jet during flow-visualization tests.

The supply tube consisted of a 2.43 m length of 6.35 mm inner-diameter stainless-steel seamless tubing giving an l/d of approximately 383. According to the equation developed by Langhaar (1942) for the laminar development length, the exit velocity profile remains parabolic for Reynolds numbers Re below 6600.

The settling chamber was connected to the supply tube by means of a bellmouth entrance section. Extreme care was taken to ream the bellmouth neck to the same size as the inner diameter of the supply tube.

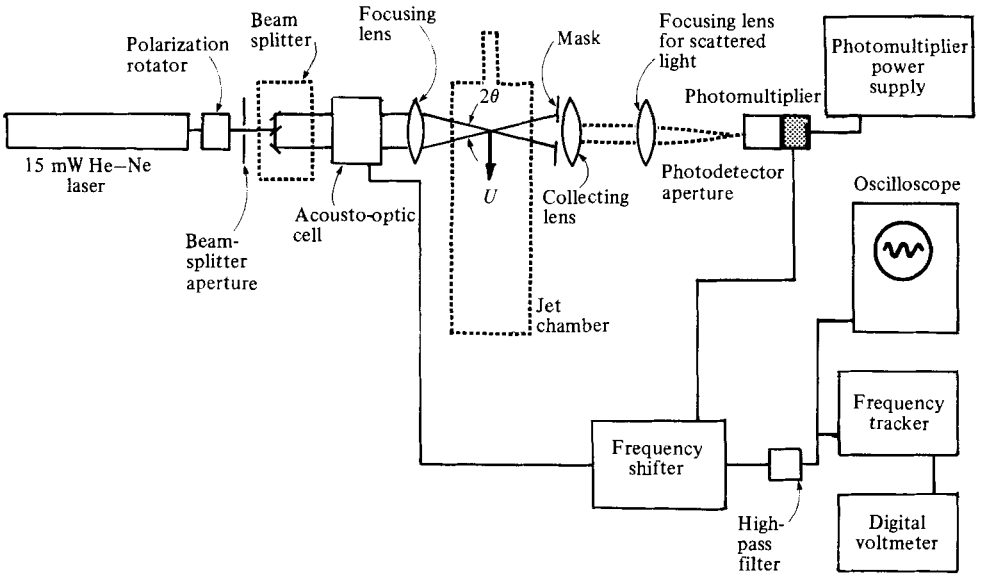

FIGURE 3. Laser-Doppler anemometer arrangement.

A schematic diagram of the dual-beam laser-Doppler anemometer arrangement that was used is shown in figure 3. The jet chamber is shown with a dashed line for reference. The He–Ne laser beam diameter was 1.1 mm between $1/e^2$ points, the focal length of the focusing lens was 102.1 mm and intersected with an included angle 2θ of 27.52°. Thus the measuring volume was approximately 0.315 mm long and 0.078 mm in diameter. With a frequency tracker sensitivity of 20 V MHz^{-1} the sensitivity of the overall instrument was 66.5 mm s^{-1} V^{-1}. The uncertainty of the velocity measurement was estimated to be ± 1 mm s^{-1}; for radial and axial positioning it was ± 0.03 mm and for mass flow rate ± 0.0001 kg s^{-1}. Further details of the experimental equipment are presented by Rankin (1980).

3. Velocity-profile measurements

The flow rate was set such that the Reynolds number was known to within 3%. A flow-visualization study was conducted to determine the laminar region of the jet. A weak solution of Meriam no. D-2930 (green) manometer fluid and water was injected into the settling chamber for this purpose. At this point the positions in the x-direction at which velocity profiles were to be taken were decided. Only axial distances well within the laminar region were chosen. Positions at which the jet boundary oscillated slightly were also excluded from consideration. The jet was traversed in the z-direction while holding y constant in order to determine the centre of the jet.

The measuring volume was then traversed in the y-direction while voltage and distance values were recorded at intervals of 0.25 mm over most of the jet. Intervals of 0.50 and 1.25 were used where velocity gradients were small.

Selected dimensionless velocity profiles are presented in figures 4–7. The radial coordinate is non-dimensionalized with the half-radius $r_{\frac{1}{2}m}$ and the velocity by the value u_m at the centreline. In order to eliminate overcrowding of data points in the figures, not all of the experimental data have been shown on these diagrams.

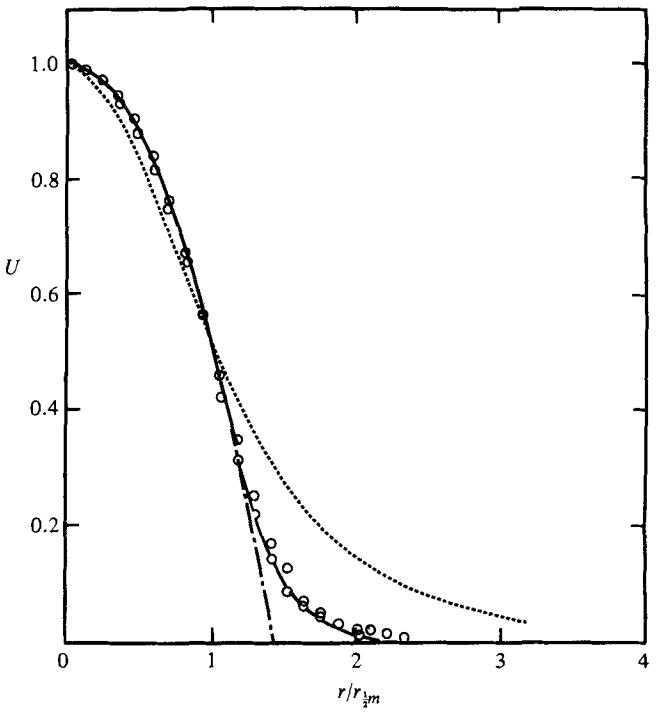

FIGURE 4. Non-dimensional axial-velocity profile, $X_c = 0.001$, $Re_c = 4000$; – – – –, Schlichting (1968); —·—, parabola; ——, Arulraja (1982).

The eliminated data in no way affect the interpretation of the results. A complete set of experimental values in tabular form is given by Rankin (1980). Samples of data from the complete velocity profile (i.e. both positive and negative values of y) are included, which in conjunction with a slight asymmetry in the velocity-profile data account for the small amount of scatter that appears. The analytical velocity profile of Arulraja (1982), the parabolic exit velocity profile, and that of Schlichting (1968) are given for comparison. The finite-difference solution of the boundary-layer equations is in excellent agreement with the data in each case.

The results for $x/d = 4$ and $Re_c = 4000$ are presented in figure 4. Such a combination of x/d and Re_c yields a value of $X_c = (x/d)\, Re_c^{-1} = 0.001$, which, according to theory, is considerably underdeveloped. This is particularly evident in the figure presented since the major portion of the jet flow field is parabolic.

Data from three different Reynolds numbers Re_c are plotted on figure 5. The x/d values are chosen such that $X_c = 0.005$ in all three cases. The fact that all the curves collapse reasonably onto one indicates that X_c is the proper non-dimensional axial coordinate with which to characterize jet development. This is in agreement with the analytical methods which make use of the boundary-layer simplifications; however, it is in disagreement with the experimental findings of Abramovich & Solan (1973).

The experimental points in the region $r/r_{\frac{1}{2}m}$ greater than unity approach Schlichting's solution. In contrast, those points in the region where $r/r_{\frac{1}{2}m}$ is less than unity fall close to the non-dimensional parabola. Arulraja, Rankin & Sridhar (1983) have used this fact to derive an approximate analytical solution for the jet centreline velocity.

It appears that, at least in a dimensionless manner, the velocity-profile adjustment from the tube conditions to the free-jet conditions takes place at the jet outer edges

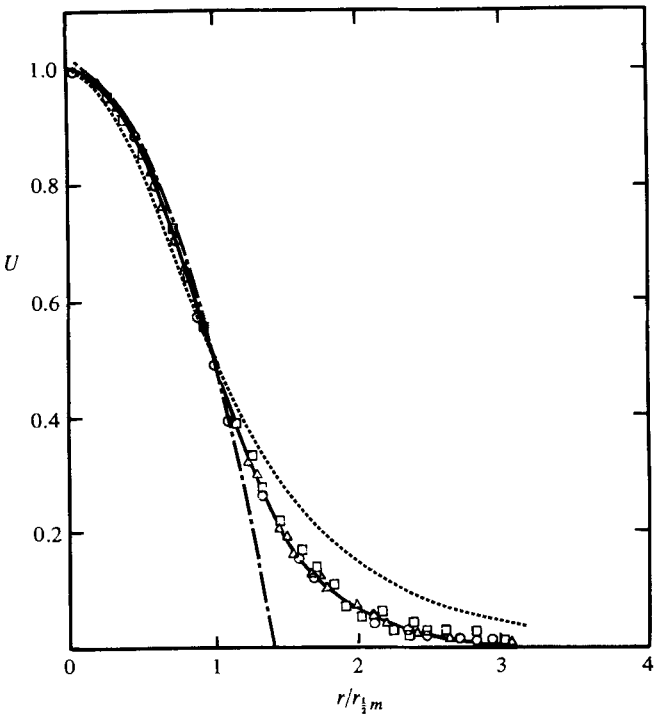

FIGURE 5. Non-dimensional axial-velocity profile; $X_c = 0.005$; ----, Schlichting (1968); —·—, parabola; ——, Arulraja (1982); ○, $Re_c = 1000$; △, 1500; □, 2000.

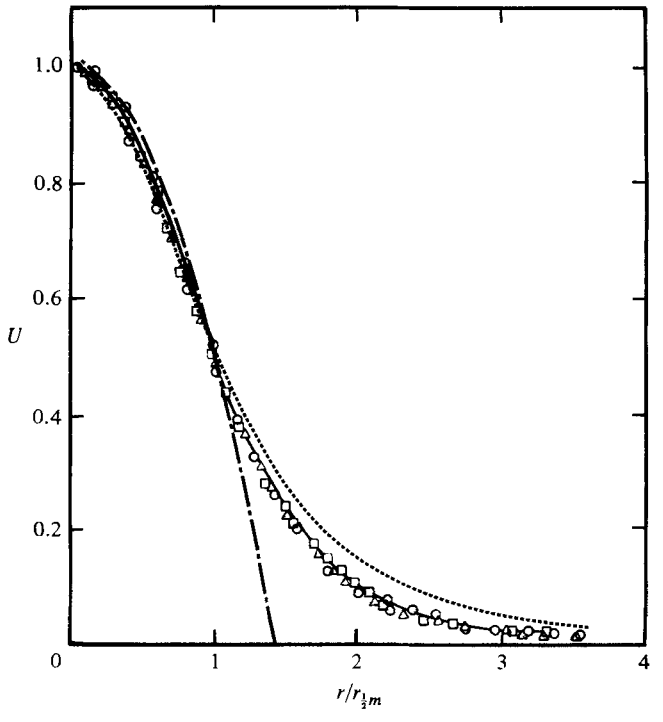

FIGURE 6. Non-dimensional axial-velocity profile; $X_c = 0.01$; ----, Schlichting (1968); —·—, parabola; ——, Arulraja (1982); ○, $Re_c = 1000$; △, 1500; □, 2000.

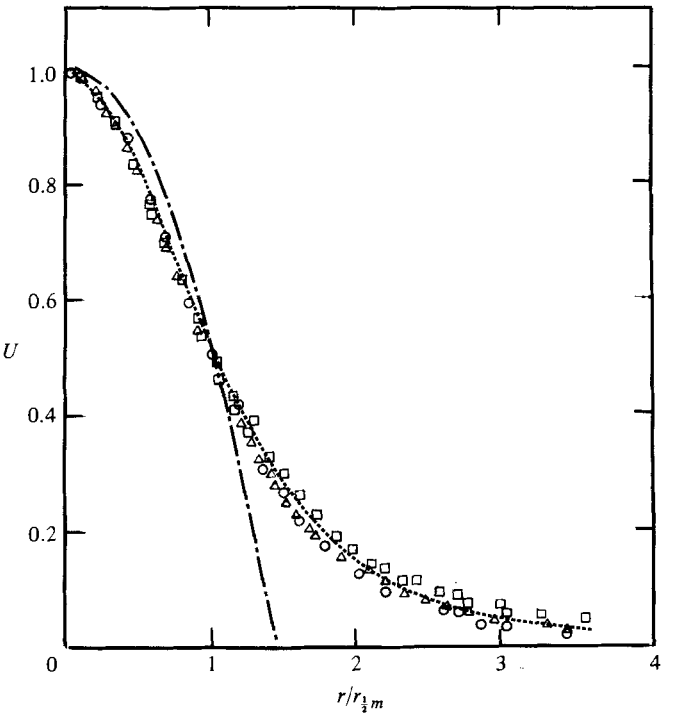

FIGURE 7. Non-dimensional axial-velocity profile, fully developed; ----, Schlichting (1968); —·—, parabola; ○, $X_c = 0.018$, $Re_c = 1500$; △, 0.025, 1000; □, 0.035, 1000.

first. Further adjustment in the outer region is evident also in the data at $X_c = 0.01$, presented in figure 6. The collapse of the experimental data and excellent agreement between theory and experiment are also apparent in this figure.

Figure 7 contains experimental data from three different X_c conditions; namely 0.018, 0.025 and 0.035. These results seem to fall reasonably close to the Schlichting velocity profile. This indicates that fully developed conditions exist. The distance can be given approximately as $X_c = 0.018$, which is in reasonable agreement with the values found in the literature.

The variation of centreline velocity with dimensionless axial distance X_c is presented in figure 8. The agreement with the analytical methods is excellent near the tube exit. Further downstream, this agreement becomes slightly less. The data possess only a small amount of scatter. A plot using the axial coordinate $X^* = (x/d)\, Re^{-\frac{1}{2}}$ is shown in figure 9. The increased scatter is a further indication that X_c is the proper non-dimensional axial coordinate. A curve has been fitted to these data points, and is also indicated on the figure. This line of best fit is used in a later section.

The jet lengthscale, namely the jet half-radius, is presented in figure 10. Again agreement with the analytical method is excellent and a curve is fitted to the data which will be used.

4. Jet momentum flux

The velocity-profile data were collected using sufficiently small radial increments so that the basic definition could be used to determine the axial momentum flux. The

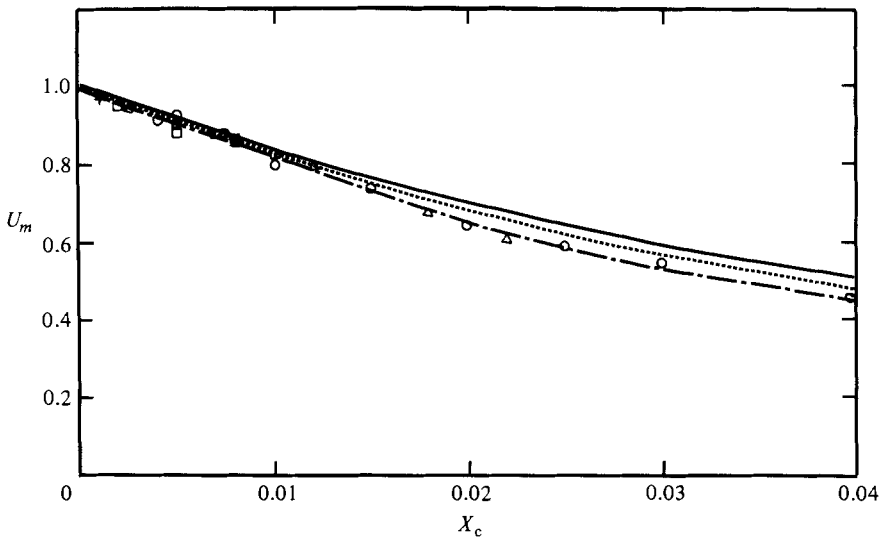

FIGURE 8. Centreline velocity variation with dimensionless axial distance X_c; —·—, line of best fit; – – –, Pai & Hsieh (1972); ——, Arulraja (1982); +, $Re_c = 4000$; □, 2000; △, 1500; ○, 1000.

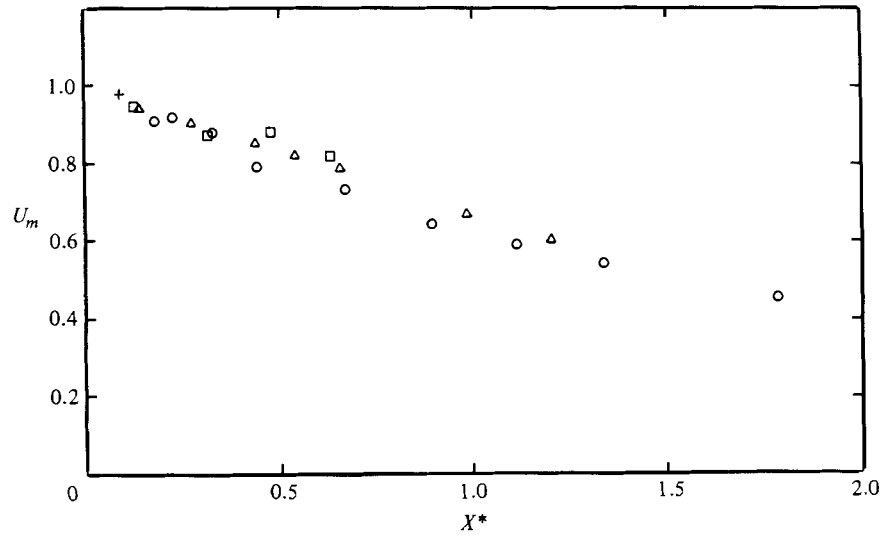

FIGURE 9. Centreline velocity variation with X^*: +, $Re_c = 4000$; □, 2000; △, 1500; ○, 1000.

kinematic momentum flux will be used here, and is defined as

$$K = \frac{J}{\rho} = 2\pi \int_0^\infty u^2 r \, \mathrm{d}r. \tag{4}$$

In order to use this definition directly, it is necessary to perform the indicated integration numerically. It is convenient to modify the equation as follows:

$$K = \pi \int_0^\infty u^2 \, \mathrm{d}(r^2). \tag{5}$$

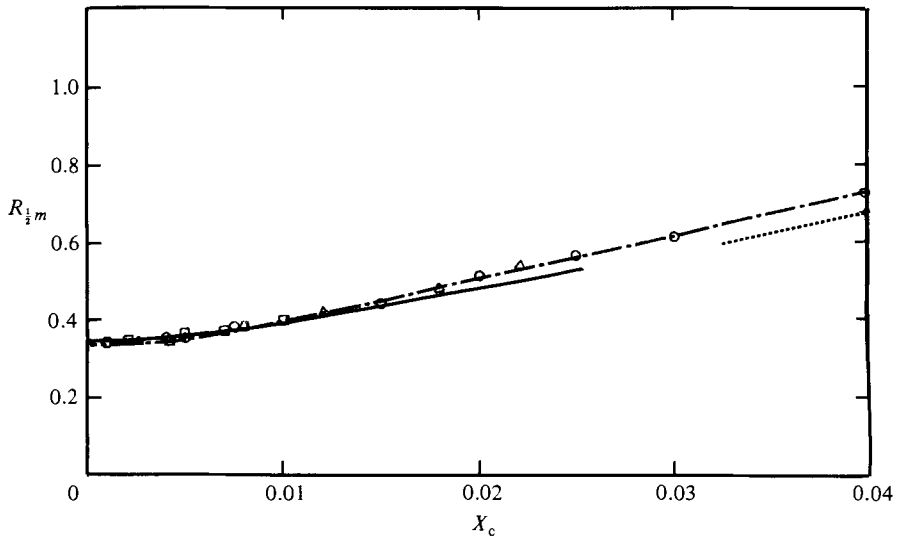

FIGURE 10. Variation of jet half-radius with dimensionless axial distance; —·—, line of best fit; – – –, Pai & Hsieh (1972); ——, Arulraja (1982); +, $Re_c = 4000$; □, 2000; △, 1500; ○, 1000.

This equation can now be approximated using the trapezoidal rule as

$$K = \pi \sum_{i=1}^{n-1} \tfrac{1}{2}(r_{i+1}^2 - r_i^2)\,(u_i^2 + u_{i+1}^2), \tag{6}$$

where n is the number of data points, r the radial coordinate and u the axial velocity component. It should also be mentioned that, in order to avoid error accumulation due to possible inaccuracies near the jet boundaries, the profile was integrated between the points where $u = 0.05u_m$. If such data points did not exist, they were generated using an interpolation procedure.

The momentum flux can be made dimensionless by dividing it by the value K_0 at the tube exit. In the case of a parabolic exit profile this value can be shown to be

$$K_0 = \tfrac{1}{12}\pi d^2 u_{\max}^2. \tag{7}$$

The value of $u_{\max}$ is determined using the mass-flow-rate information. A plot of the variation of K/K_0 with axial distance is shown on figure 11. The common assumption that the momentum is conserved is represented by a horizontal line through $K/K_0 = 1$ on this plot. Although scatter of the data is considerable, a general trend seems to be evident which indicates an initial decrease in K/K_0 followed by an increase to a value greater than unity. A constant value is reached far downstream.

One reason for the spread of the data in figure 11 can be readily seen by considering (5), rearranged as follows:

$$K = \pi r_{\frac{1}{2}m}^2 u_m^2 \int_0^\infty \left(\frac{u}{u_m}\right)^2 \mathrm{d}\left(\frac{r}{r_{\frac{1}{2}m}}\right)^2$$

$$= \pi r_{\frac{1}{2}m}^2 u_m^2 \beta, \tag{8}$$

and non-dimensionally as

$$\frac{K}{K_0} = 8R_{\frac{1}{2}m}^2 U_m^2 \frac{\beta}{\beta_0}, \tag{9}$$

where $\beta_0 = \frac{2}{3}$ for a parabolic exit velocity profile. This equation shows that K/K_0

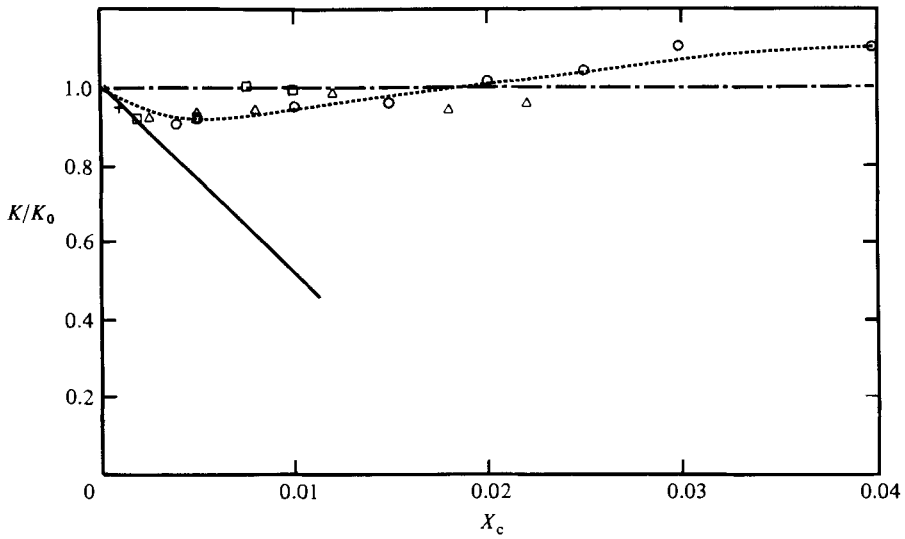

FIGURE 11. Variation of momentum ratio with dimensionless axial distance; ----, line of best fit; ——, $K/K_0 = 1\text{–}48X_c$; —·—, common assumption; +, $Re_c = 4000$; □, 2000; △, 1500; ○, 1000.

depends on three quantities: the half-radius $r_{\frac{1}{2}m}$; the local maximum velocity u_m, and a non-dimensional integrated value β which is referred to as a momentum flux coefficient. Each of these quantities is determined with some degree of uncertainty and they are combined to yield a quantity which is more uncertain. A method of obtaining K/K_0 with less uncertainty is to arrive at the values in (9) separately, before combining. Curves of $R_{\frac{1}{2}m}$ $(=r_{\frac{1}{2}m}/d)$ and U_m $(=u_m/u_{\max})$ versus X_c have been obtained by curve-fitting the data to accomplish this. The goodness of fit of these curves is evident in figures 8 and 10.

A plot of β/β_0 versus X_c is presented in figure 12. The degree of scatter of this quantity is considerably less than that of K/K_0 versus X_c. It is also noticed that this curve seems to indicate a development length longer than that mentioned previously. A curve was fitted to this data in a manner similar to that of U_m and $R_{\frac{1}{2}m}$, and is shown on the diagram. The curves mentioned above were used in conjunction with (9) to plot the dashed line in figure 11. The trend that this line indicates has two aspects which are particularly interesting. One is the increase in momentum far downstream. This observation is in contrast with that of Abramovich & Solan (1973), who noticed a decrease in momentum. The possibility of an increase in momentum is certainly a point that one may question. It should be mentioned that such an increase in momentum has been reported in certain turbulent-jet studies. Hussain & Clark (1977) report increases by as much as 20–56 % over the tube exit value. They attempt to account for this increase by considering the influence of static pressure changes. Pressure forces will also be considered in what follows.

A cylindrical control volume is chosen as shown in figure 13(*a*). It completely includes the developing region of the jet and is infinite in radial extent. The x-component of the momentum theorem applied to this control volume yields the following equation:

$$\int_\infty \left(\frac{P}{\rho}\mathrm{d}A\right)_0 - \int_\infty \left(\frac{P}{\rho}\mathrm{d}A\right)_\mathrm{d} = -\int_\infty (u^2\,\mathrm{d}A)_0 + \int_\infty (u^2\,\mathrm{d}A)_\mathrm{d}. \tag{10}$$

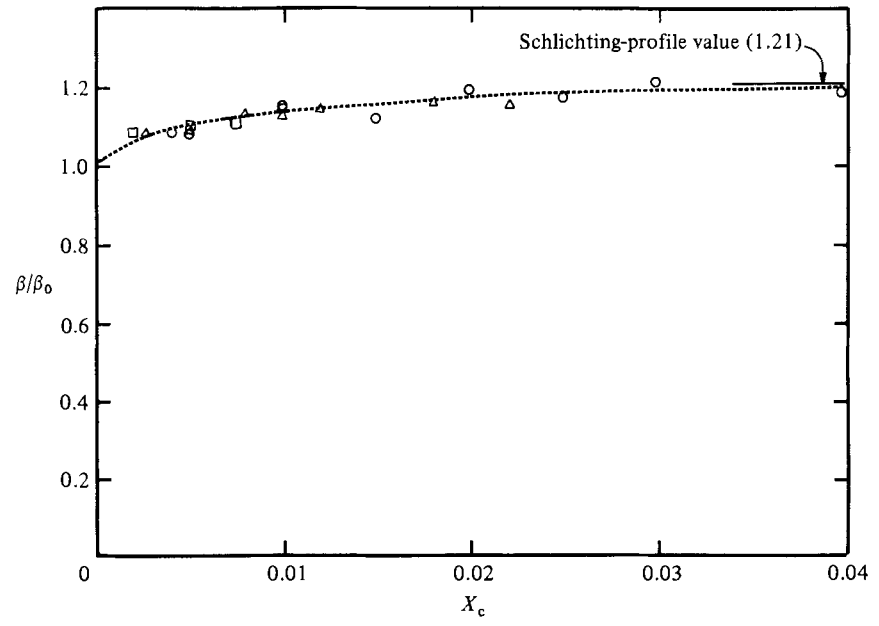

FIGURE 12. Momentum-flux coefficient variation with axial distance; ----, line of best fit; +, $Re_c = 4000$; □, 2000; △, 1500; ○, 1000.

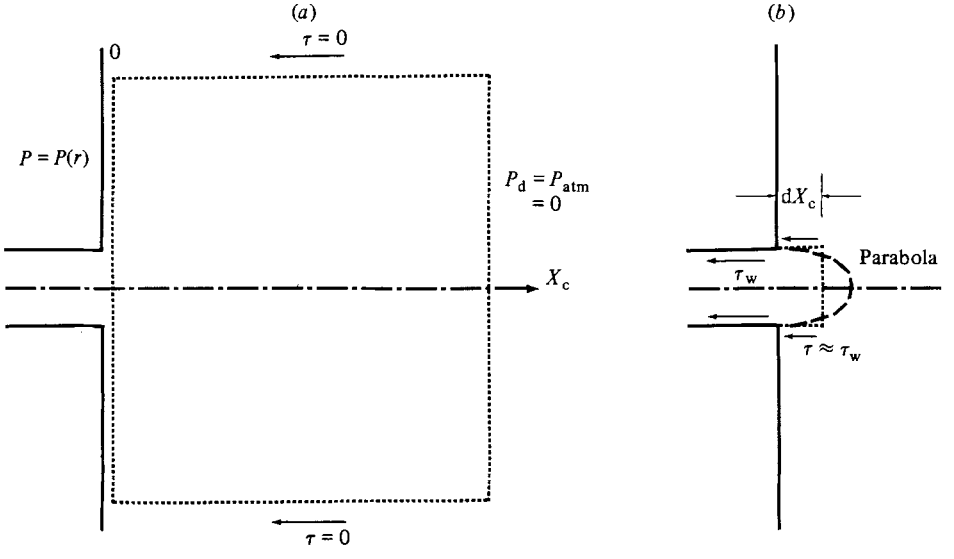

FIGURE 13. Control volumes selected for analysis.

The subscripts 0 and d refer to planes, perpendicular to the jet axis, at the exit of the jet and within the fully developed region respectively. Denoting the pressure force as F and the kinematic momentum as K, using the same subscripts as above, the equation reduces to

$$\frac{F_0 - F_d}{\rho} = -K_0 + K_d. \tag{11}$$

However, the (gauge) pressure forces on planes within the fully developed region must

be zero, and therefore

$$\frac{K_d}{K_0} = \frac{F_0}{\rho K_0} + 1. \tag{12}$$

The pressure force on the solid bounding surface need not be zero. This equation indicates that the ratio K_d/K_0 can be greater than unity if the pressure force across the exit plane is positive. Such a condition could occur if the pressure within the supply tube does not reach the atmospheric value at the exit of the tube. Then the pressure adjustment must occur outside of the tube. This is a hypothesis which is yet to be verified experimentally.

The second point of interest on this graph is the initial decrease of the momentum ratio. Consider the control volume shown in figure 13(*b*). This control volume is equal in diameter to the supply tube, and its thickness is infinitesimally small. Assuming that the gradient of pressure is approximately zero at the exit of the tube the non-dimensional momentum equation for steady flow applied to the control volume is

$$\frac{d(K/K_p)}{dX_c} = -\frac{24}{\mu}\frac{R\tau}{u_{max}}. \tag{13}$$

Assuming that a parabolic velocity profile exists at the tube exit, the velocity gradient at the edge of the control volume may be approximated as that of a parabola because of the small thickness of the control volume. Therefore

$$\tau = \frac{2\mu u_{max}}{R}, \tag{14}$$

and hence

$$\left.\frac{d(K/K_0)}{dX_c}\right|_{X_c=0} = -48. \tag{15}$$

This equation gives the slope of the curve in figure 11 at $X_c = 0$, and appears to be in good agreement with the data. This result seems more reasonable when it is considered that the velocity profiles must approach a parabolic shape as the distance downstream tends to zero. A careful study of this diagram reveals the fact that only a few data points are available very close to the tube exit. Additional information is needed in this region to evaluate properly the accuracy of the above method of predicting the initial decrease in the momentum. Data were taken in the range $0 < X_c < 0.1$ using a laser-Doppler anemometer in the reference-beam mode. This mode allowed the measuring volume to be placed closer to the tube exit (within 2 mm) than with the dual-beam mode. Lens focal lengths and other pertinent data including data-reduction methods remained the same. The variation of K/K_0 with X_c is shown on figure 14 along with the straight-line approximation to the slope at $X_c = 0$ and the original data that fall within this range. The new momentum data decrease more rapidly than the values predicted using the simple assumptions. The general trend of the variation is, however, similar to that of the previous experiments, considering the scatter of the data.

5. Conclusions

The experimental velocity field of the laminar axisymmetric submerged jet issuing from a long tube compares quite favourably with solutions of the equations of motion subjected to the usual boundary-layer simplifications, both in the developing and fully developed regions. This indicates that the proper non-dimensional axial coordinate required to collapse the experimental data is $(x/d)\,Re_c^{-1}$. The common

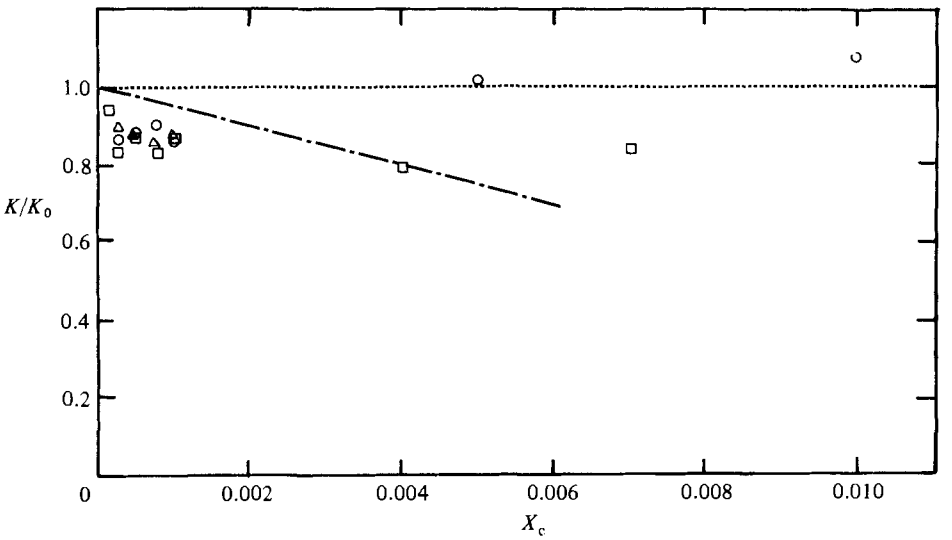

FIGURE 14. Variation of momentum ratio for small values of axial distance; ----, common assumption; —·—, $K/K_0 = 1-48X_c$; △, $Re_c = 4000$; □, 2000; ○, 1000.

assumption of conservation of momentum is only a reasonable approximation. Momentum appears to decrease initially upon exiting the tube and then gradually increases until at large distance downstream it reaches a constant value which is greater than that in the supply tube. The general trend of the variation can be partially explained by making certain simplifying hypotheses regarding conditions of the velocity profile, pressure and shear stress at the jet exit.

The authors wish to thank the Research Board of the University of Windsor for their financial support and the Natural Sciences and Engineering Research Council Canada for their financial support through Grant Numbers A-2190, A-1403 and E-5381. The assistance rendered by Mr R. Tattersall and Mrs B. Carr is gratefully acknowledged.

REFERENCES

ABRAMOVICH, S. & SOLAN, A. 1973 The initial development of a submerged laminar round jet. *J. Fluid Mech.* **53**, 791–801.

ANDRADE, E. N. & TSIEN, L. C. 1937 The velocity distribution in a liquid into liquid jet. *Proc. Phys. Soc. Lond.* **49**, 381–391.

ARULRAJA, M. 1982 Analysis of developing region of a submerged laminar free jet. M.A.Sc. thesis, University of Windsor.

ARULRAJA, M., RANKIN, G. W. & SRIDHAR, K. 1983 Maximum velocity decay in a submerged laminar jet issuing from a long tube. *Trans. Can. Soc. Mech. Engng* **7**, 41–43.

BIRKHOFF, G. & ZARANTONELLO, E. H. 1957 *Jets, Wakes and Cavities.* Academic.

CHANG, H. 1972 An analytical and experimental investigation of a large-scale model of a turbulence amplifier. M.Sc. thesis, SUNYAB.

DMITRIEV, V. N. & KULESOVA, N. A. 1974 The calculation of a laminar jet in the surroundings of the supply nozzle. In *Proc. 5th Jablonna Fluidics Conf., Budapest.*, 83–91, M/S KULTURA.

DU PLESSIS, M. P., WANG, R. L. & TSANG, S. 1973 Development of a submerged round laminar jet from an initially parabolic profile. *Trans. ASME* G: *J. Dyn. Syst. Meas. & Control* **95**, 148–154.

FOX, H., SINHA, R. & WEINBERGER, L. 1972 An implicit finite difference solution for jet and wake problems. *Astronautica Acta* **17**, 265–278.

HRYCAK, P., LEE, D. T., GAUNTER, J. W. & LIVINGOOD, J. N. B. 1970 Experimental flow characteristics of a single turbulent jet impinging on a flat plate. *NASA TN* D-5690.

HUSSAIN, A. K. M. F. & CLARK, A. R. 1977 Upstream influence on the near field of a plane turbulent jet. *Phys. Fluids* **20**, 1416–1426.

LANDAU, L. D. 1944 A new exact solution of the Navier–Stokes equations. *C.R. Acad. Sci. URSS* **43**, 286–289.

LANGHAAR, H. L. 1942 Steady flow in the transition length of a straight tube. *J. Appl. Mech.* **10**, 55–58.

MORTON, B. R. 1967 Entrainment models for laminar jets, plumes and wakes. *Phys. Fluids* **10**, 2120–2127.

PAI, S. I. & HSIEH, T. 1972 Numerical solution of laminar jet mixing with and without free stream. *Appl. Sci. Res.* **27**, 39–62.

RANKIN, G. W. 1980 Developing region of laminar jets. Ph.D. dissertation, University of Windsor.

SCHLICHTING, H. 1968 *Boundary Layer Theory.* McGraw-Hill.

SQUIRE, H. B. 1951 The round laminar jet. *Q. J. Mech. Appl. Maths* **4**, 321–329.

SYMONS, E. P. & LABUS, T. L. 1971 Experimental investigation of an axisymmetric fully developed laminar free jet. *NASA TN* D-6304.

VAZ, T. 1970 An experimental investigation into the response of a turbulence-type amplifier and laminar/turbulent jet study. M.A.Sc. thesis, University of Windsor.